PCCP

The Potential Energy Profile of the Decomposition of 1,1-Diamino-2,2-dinitroethylene (FOX-7) in Gas Phase

Journal:	*Physical Chemistry Chemical Physics*
Manuscript ID	CP-ART-08-2022-003719.R1
Article Type:	Paper
Date Submitted by the Author:	02-Oct-2022
Complete List of Authors:	Luo, Yuheng; University of Hawai'i at Manoa Kang, Christopher; University of Hawai'i at Manoa, Chemisty Kaiser, Ralf; University of Hawaii, Sun, Rui; University of Hawai'i at Manoa, Chemisty

ARTICLE

The Potential Energy Profile of the Decomposition of 1,1-Diamino-2,2-dinitroethylene (FOX-7) in Gas Phase

Received 00th January 20xx,
Accepted 00th January 20xx

DOI: 10.1039/x0xx00000x

Yuheng Luo,[a] Christopher Kang,[a] Ralf Kaiser [a,b] and Rui Sun *[a]

1,1-Diamino-2,2-dinitroethene (FOX-7) is an energetic material with low sensitivity and high detonation performance, thus it has been considered as a potential replacement for traditional nitro-based energetic materials. In a recent publication (J. Phys. Chem. A, 2022, 126, 4747), the initial decomposition steps of FOX-7 were studied with reflectron time-of-flight mass spectrometry and infrared spectroscopy. The experimental study was complemented with quantum chemistry calculations, which demonstrated the gas phase potential energy surface to be indicative of the reaction process in the condensed phase. The computation in J. Phys. Chem. A, 2022, 126, 4747 focuses on the primary decomposition – but in this manuscript, the full decomposition pathway on the singlet surface, consisting of 54 intermediates and 37 transition states, is characterized at an unprecedented detail. The calculations show that the nitro group, instead of the amine group, is primarily responsible for the sensitivity and endothermicity of FOX-7 decomposition. This result sheds light on how to critically optimize the performance of FOX-7 and design the next generation of nitro-based energetic materials. A comprehensive roadmap, initiated from FOX-7, covers the chemical space of the entire decomposition thus providing a holistic demonstration of various key decomposition pathways leading to various small, gas phase products such as NO, NO_2, NH_2, CO_2, and CO.

I. Introduction

1,1-Diamino-2,2-dinitroethene (FOX-7) is a highly energetic material with low sensitivity[1–5] and it has attracted scientists' attention since first synthesized in 1998[6]. Currently, the commonly used explosives such as cyclo-1,3,5-trimethylene-2,4,6-trinitramine (RDX) features high detonation performance[7] and simple synthesis procedure[8], while suffering from high sensitivity to heat, impact, and friction[9], presenting certain challenges to storage, transportation, and operation. FOX-7 has been reported to be insensitive to those stimuli and exhibits a comparable level of detonation performance thus is deemed as a potential replacement for RDX.[10–12] Therefore, understanding the reaction mechanisms involved in the initial decomposition and successive reactions of the carbon, nitrogen, and oxygen-centered radicals formed in the decomposition of FOX-7 is important to realize its full potential.

The decomposition of FOX-7 has been studied with quantum chemistry calculations in the past decade.[13–19] The molecular geometry and decomposition energy of FOX-7 was first calculated by Politzer et al.[13] using the density functional theory (DFT) functional B3P86[20,21] and 6-31+G(d,p)[22] basis set. The energies of C-NO_2 and C-NH_2 bond cleavage were reported to be 293 and 467 kJ/mol, respectively. These two bond rupture processes were confirmed as a barrierless process by Kimmel et al.[15] using the B3LYP[23] functional with 6-31+G(d,p) basis set. The relative energies of initial decomposition products reported by various research are summarized in Table 1.

Table 1. Relative energies (kJ/mol) of initial decomposition pathways of FOX-7. The structure of species can be found in Figure 1.

Geometry	B3P86 6-31+G(d,p)	B3LYP 6-31+G(d,p)	MP2[d] 6-31G(d)	B3LYP[e] 6-311++G(3df,2p)	M06-2X[f] 6-311++G(2df,p)	M06-2X-D3[g] Def2-TZVPP	**M06-2X-D3[g] Def2-TZVPP**
Energy	B3P86 6-31+G(d,p)	B3LYP 6-31+G(d,p)	MP2 6-31G(d)	G4 6-311++G(3df,2p)	CCSD(T)-F12B AVTZ-F12	M06-2X-D3 Def2-TZVPP	**CCSD(T)-F12A VTZ-F12**
TS1	249[b]	247[b], 266[c]	251	244	252	293	**273**
I4 + NO	2[b]	-28[b], -28[c]		-19	-23	-23	**-15**
I6 + NO2	293[a], 288[b]	263[b], 280[c]	318	290	301	302	**300**
I7 + NH2	467[a]	464[c]	469			466	**461**

[a]: Ref. 13, [b]: Ref. 14, [c]: Ref. 15, [d]: Ref. 16, [e]: Ref. 17, [f]: Ref. 18, [g]: Ref. 19

[a] *Department of Chemistry, University of Hawaii, Honolulu, HI 96822, USA.*
[b] *W. M. Keck Research Laboratory in Astrochemistry, University of Hawaii, Honolulu, HI 96822, USA.*
* Corresponding Authors: ruisun@hawaii.edu.

The dissociation of nitric oxide (NO) *via* nitro-to-nitrite rearrangement was reported by Gindulyte et al.[14] using two DFT functionals (B3P86 and B3LYP) with 6-31+G(d,p) basis set. The transition state (TS) was located about 250 kJ/mol above FOX-7 and was lower than the barrier previously found[13] for the nitrogen dioxide (NO_2) dissociation pathway. The TS yielded a metastable nitrite isomer, followed by NO loss, which was nearly isothermic. The remaining radical $(H_2N)_2CC(O)NO_2$ underwent H-shift and then decomposed to $H_2N(NH)CCO$ radical and nitrous acid (HONO). The $H_2N(NH)CCO$ radical would further decompose into carbon monoxide (CO), hydrogen isocyanide (HNC), and amino radical (NH_2) *via* two subsequent decomposition steps. This study for the first time revealed the nitro-to-nitrite rearrangement to be an important initial decomposition step of FOX-7, although the relative energies were not reliable due to large differences observed in two different DFT methods (e.g., The overall barrier from FOX-7 to the final products is 290 kJ/mol from B3LYP and 392 kJ/mol from B3P86). Booth and Butler explored more initial and subsequent thermal decomposition pathways of FOX-7 in the gas phase. The authors refined the energy with G4 method[24] after obtaining the molecular geometry at the B3LYP/6-311++g(3df,2p)[22] level. This work confirmed the nitro-to-nitrite isomerization but reported a new transition state connecting the nitrite isomer $(H_2N)_2CC(ONO)NO_2$ and the NO loss product $(H_2N)_2CC(O)NO_2$. A new NO_2 loss pathway *via* an intramolecular H-shift transition state and isomer $H_2N(NH)CC(NO_2)_2H$ was also discovered. The authors also explored subsequent decompositions, yielding various gas phase products such as hydroxyl radical (OH), atomic hydrogen (H), CO and carbon dioxide (CO_2). However, some of the decomposition pathways missed certain key structures and ended too early before forming stable, small gas products, especially those initiated from $(H_2N)CC(NO_2)_2$, which is one of the important initial decomposition (NH_2 loss) pathways of FOX-7.

The previous computational studies on gas-phase FOX-7 have also shown some conflicting results. For example, Gindulyte et al.[14], Kiselev and Gritsan[18], and Turner et al.[19] suggested NO emits from the nitrite isomer (after the nitro-to-nitrite isomerization) with a barrier of less than 10 kJ/mol, while Booth and Butler[17] reported a CO-NO bond rupturing transition state locating 61 kJ/mol above the nitrite isomer, and Guan et al.[25] reported a transition state locating 43 kJ/mol above the nitrite isomer, which is followed by a hydrogen-bonded intermediate before NO loss. Further, most of the previous works were done at the DFT or second order Møller-Plesset perturbatbion theory (MP2)[26] level – with proper basis sets, these methods can be expected to give quantitatively accurate molecular geometries (e.g., within 0.015 Å error in bond lengths).[27] However, these methods only give qualitatively reliable potential energies, including an uncertainty of a few kJ/mol in reaction energies and tens of kJ/mol in TS heights.[28] As shown in Table 1, the DFT methods have comparatively a larger error (in comparison to explicitly correlated coupled-cluster method with single and double excitations and a perturbative treatment of triple excitations (CCSD(T)-F12)[29]) at transition state (**TS1**) than intermediates (**I4** + NO, **I6** + NO_2, and **I7** + NH_2). In a recent work, the authors' group refined the single-point potential energy of the structures found using DFT with CCSD(T)-F12 and showed success in accurately representing barriers and energies of the initial decomposition steps of FOX-7, which was verified by their agreement to experiment.[18,19] The combination of the low-cost DFT method and the highly accurate CCSD(T)-F12 method balances the efficiency and accuracy of quantum chemistry calculation, thus it is employed in this study.

This manuscript seeks to portray a more comprehensive and accurate picture of the decomposition pathways of gas-phase FOX-7. A few interesting isomerization mechanisms, such as NO and NO_2 groups migrating from one carbon to another, and an unconventional pathway triggered by a nitro-to-nitrite TS lookalike are discovered from this study. Although FOX-7 is synthesized and employed in the condensed phase, as demonstrated in other research, the study on decomposition in the gas phase is still indicative and sheds light on the reaction in the condensed phase.[19,30–33]

II. Computational methodology

The decomposition pathways of FOX-7 are investigated starting from a monomolecular structure in the gas phase. All stationary points (FOX-7, intermediates, transition states, and products) are optimized with dispersion-corrected density functional theory (DFT-D3) M06-2X-D3[34,34]/def2-TZVPP[35] in NWChem (Version 6.8.1)[36], which has been proven to give accurate structures for the titled reaction[19]. Vibrational frequency calculations with the same methods are carried out to confirm the validity of stationary points (e.g., stationary points have 3*N*-6 vibrational modes with a positive frequency; transition states have 3*N*-7 vibrational modes with a positive frequency and 1 vibrational mode with an imaginary frequency, where *N* is the number of atoms). The unscaled zero-point energy (ZPE) is computed according to the vibrational frequencies. In addition, the connections between transition states to intermediates are carefully verified with intrinsic reaction coordinate (IRC)[37–39] calculations. In some cases where IRC calculations encounter a shoulder (e.g., potential energy stop decreasing further as the geometry updates), finer IRC steps and/or re-optimization are performed. Whether a barrier (i.e., TS) exists between an intermediate and its respective separated molecules is analyzed following the procedures from recent studies: the dissociated molecules are separated by 10 + Å and aligned to resemble the target intermediate. The system is allowed to relax following the energy gradient.[40,41] The dissociation of a target intermediate to separated molecules will be considered barrierless if both the distance and the potential energy of the system monotonically decrease until the system configuration relaxes to the target intermediate. Natural bond orbital (NBO) analysis[42–44] is carried out by Mayer bond order extension[45] compiled in Multiwfn (Version 3.8)[46] to analyze the bond order and bond strength.

The energies of all stationary points are refined using the CCSD(T)-F12A/cc-pVTZ-F12[29,47–49] in Molpro (Version

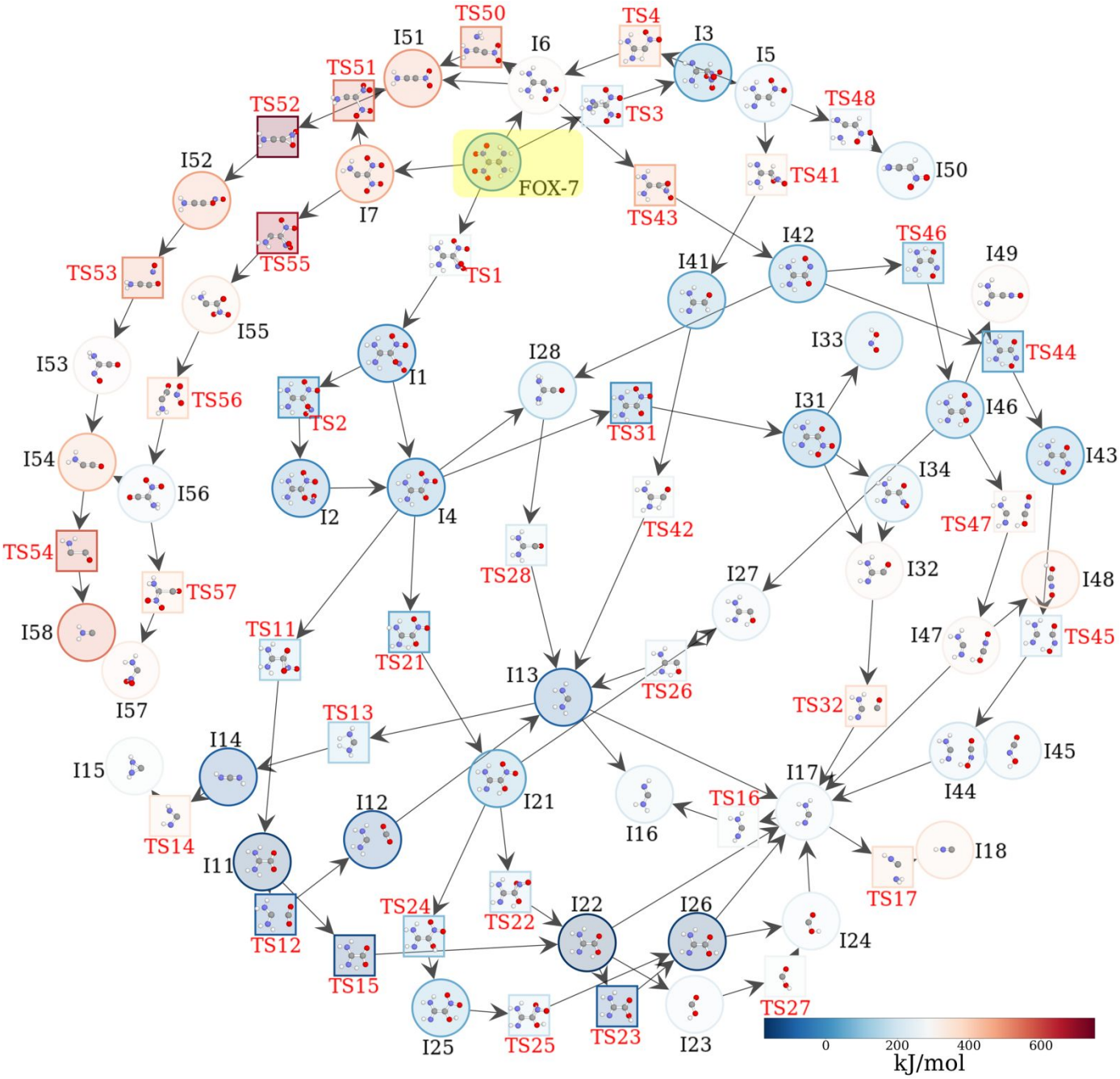

Figure 1 The decomposition map of FOX-7, which stems from the gas-phase of FOX-7 (highlights in yellow) and ends at various small products. Intermediates and products are labelled as "**I**" in black, and their structures are placed into round boxes; the transition states are labelled as "**TS**" in red, and their structures are placed into square boxes. The color of the box indicates the potential energy of the system with zero-point energy correction. The arrow denotes a decomposition or an isomerization process. Common gas phase molecules such as NO, NO_2, CO_2. are not included in the map.

2021.2)[50,51]. With the built-in acceleration functions such as density fitting (DF)[52] and resolution of the identity (RI) approximations[53] in Molpro, the computational expense of CCSD(T)-F12/cc-pVTZ-F12 is slightly higher than CCSD(T)/cc-pVTZ[54], while the accuracy is at the same level of CCSD(T) with completed basis set (CBS) limit[55]. The selection of CCSD(T)-F12A instead of CCSD(T)-F12B is guided by the study[49] which states that F12A correction performs better than F12B when accompanied by triple-zeta basis sets. The potential energy profile characterized by CCSD(T)-F12A/cc-pVTZ-F12//M06-2X-D3/def2-TZVPP level of theory has shown excellent agreement to experiments in the initial decomposition step of FOX-7.[19]

III. Results

Figure 1 demonstrates a map of the decomposition pathways of FOX-7. In general, the further away the molecule gets from FOX-7, the smaller the molecule is (*via* decomposition, following the direction of the arrows). The pathways are found by attempting to break the chemical bonds that yield smaller fragments of

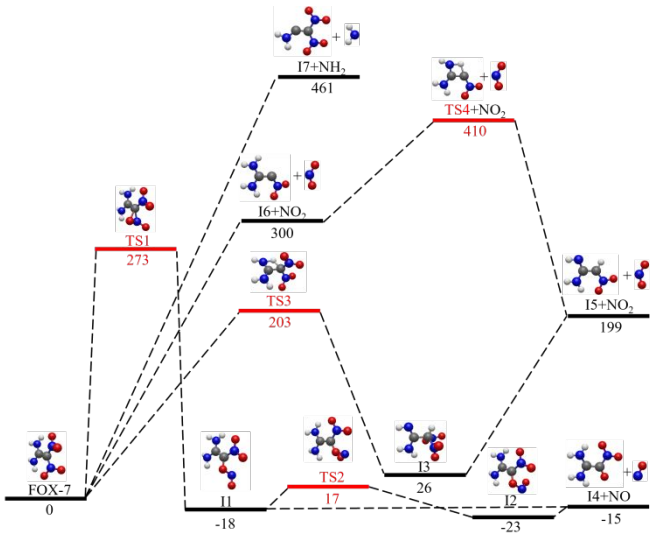

Figure 2 . The potential energy profile of the initial decomposition pathways of FOX-7 calculated at the CCSD(T)-F12/VTZ-F12A//M06-2X-D3/Def2-TZVPP + ZPE(M06-2X-D3/Def2-TZVPP) level of theory. Intermediates and products are labelled as "**I**" in black, and the transition states are labelled as "**TS**" in red.

molecules. We note that for the conciseness of the map, the intermediates listed are not exhaustive, but focusing only on those that have different atom connections. For example, only one of the *cis*- and *trans*- conformers is shown as an example, unless both lead to distinctive decomposition pathways.

The potential energy profile of initial decomposition pathways of FOX-7 has been reported in the recent experiment-computation combined study carried out by the authors' group[19] and summarized in Figure 2. There are four initial decomposition pathways starting from FOX-7: A). in a nitro-to-nitrite process, FOX-7 can isomerize to **I1** (-18 kJ/mol) *via* a cyclic transition state with a three-member ring cyclic **TS1** (273 kJ/mol). **I1** can either dissociate to a planar product **I4** (C_s) and NO, or isomerize to **I2** *via* a low transition state TS2 of 35 kJ/mol (by rotating the CO-NO bond) and then dissociate to the same products **I4** and NO. B). The cleavage of the C-NH_2 bond of the amine group yields **I7** and an amino radical NH_2 in an endothermic process of 461 kJ/mol. C). the hydrogen in the amine group can shift to the farther carbon and form **I3** after overcoming a barrier of 203 kJ/mol. One of the nitro groups in **I3** will leave and yields **I5** and NO_2. d) Another NO_2 dissociation product, **I6**, could be formed as a result of barrierless dissociation of the C-NO_2 bond in FOX-7. This process is endothermic of 300 kJ/mol. It is interesting to note that the departure of the nitro group leaves one unpaired electron to carbon, which attracts the nearby hydrogen in the amine group and triggers the interconversion of **I6** to **I5**. The further decomposition of these four primary decomposition products (i.e., **I4**-**I7)** is the focus of this manuscript. The detailed pathways initiated from each of them are demonstrated in Figures 3, 5, and 6. It is also important to note that in addition to **I4**-**I7**, the authors' group reported another initial pathway as a result of intersystem crossing[19] that releases triplet O_2 and triplet $(NH_2)_2CC(NO)_2$. Since this manuscript focuses on the decomposition taking place on the singlet surface, this pathway is beyond its scope.

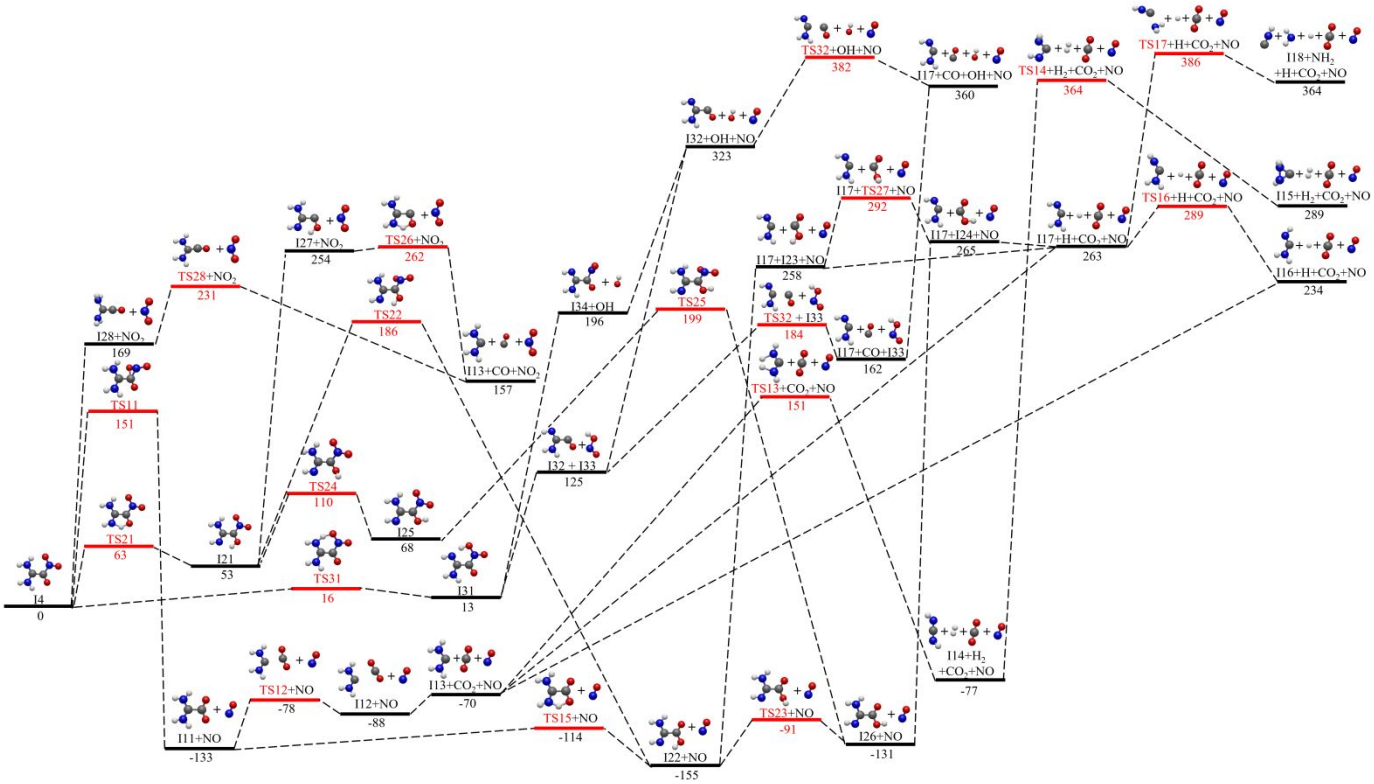

Figure 3 The potential energy profile of the subsequent decomposition pathways of gas-phase FOX-7 initiated from **I4** calculated at the CCSD(T)-F12/VTZ-F12A//M06-2X-D3/Def2-TZVPP + ZPE(M06-2X-D3/Def2-TZVPP) level of theory. Intermediates and products are labelled as "**I**" in black, and the transition states are labelled as "**TS**" in red. The initial decomposed product NO is omitted in this figure, and the potential energy of **I4** is set to zero.

A. Subsequent decomposition pathways of (the NO loss product) I4

The potential energy profile of the subsequent decomposition pathways of **I4** is detailed in Figure 3. For clarity, the potential energy of **I4** is set to zero in this figure.

After an NO loss following a nitro-to-nitrite isomerization of FOX-7, the remaining nitro group of **I4** can also form a three-member ring cyclic transition state (**TS11**) with a much smaller barrier than **TS1** (151 kJ/mol vs. 273 kJ/mol). This difference could be partially due to the increase in partial charge of the central carbon atom (+0.15 in **I4**, -0.06 in FOX-7), which attracts the electron negative oxygen to promote the ring formation. Unlike **TS1**, where after the nitro-to-nitrite isomerization (**TS1**), a post-reaction complex (**I1**) is present before eventually dissociating to **I4** and NO, **TS11** does not isomerize to a nitrite intermediate. Instead, the IRC calculation shows that the C-N and O-N bonds in **TS11** break simultaneously, and NO can be immediately formed together with a planar molecule, **I11**, $(NH_2)_2C{=}CO_2$. NBO analysis of **I11** shows that the bond orders (BO) of C-NH_2, C-O, and C-C are 1.41, 1.82, and 0.85, respectively, indicating that the π electrons of carbon atoms delocalize across the amine groups and the carboxylate group. This effect weakens the C-C bond in **I11**, thus the barrier of breaking the bond is low – **TS12** is only 55 kJ/mol higher than **I11**. **TS12** is followed by a low post-reaction complex, **I12**, before dissociating to CO_2 and **I13**, $(NH_2)_2C$ (methanediamine, C_{2v} symmetry and singlet spin state). The IRC calculation initiated from **TS12** demonstrates the validity of **I12**, which is a hydrogen-bond complex as shown in Figure 4, the entire process contains two steps – In the first step (**I11** → **I12**), one of the hydrogen bonds (H--O) breaks (2.10 Å → 4.11 Å), the C-C bond breaks (1.59 Å → 2.84 Å), while the remaining hydrogen bond is weakened (2.10 Å → 2.32 Å). During the second step, the weakened hydrogen bond breaks, which leads to dissociation between **I13** and CO_2. Previous research[17] has reported that the decomposition of **I11** has a very similar barrier of 53 kJ/mol, but it breaks the C-C bond without the postreaction complex. We note that in Ref. 17, no dispersion correction is applied thus the loosely bonded intermediate **I12** could have been missed. The two hydrogens on the side of **I13** can further leave simultaneously *via* a high energy barrier of 221 kJ/mol (**TS13**) and yield H_2 and **I14**, HNCNH (carbodiimide, C_2 symmetry). The heavy atoms in **I14** can bend and form a three-member ring product **I15** *via* another high-energy barrier (**TS14**, 441 kJ/mol). Moreover, **I13** can undergo hydrogen loss, forming **I16** + H or **I17** + H. **I16** and **I17** ($HNCNH_2$) are trans-/cis isomers and close in energy, which could convert to one another via transition state **TS16**. **I16**/**I17** could further decompose – take **I17** as an example, it can decompose into hydrogen isocyanide (**I18**) and NH_2 *via* a barrier of 123 kJ/mol (**TS17**). The overall barrier of **I4** → **I18** + NH_2 + H + CO_2 + NO is 386 kJ/mol. The pathways following **TS11** highlight several low potential energy intermediates (**I11**, **I12**, **I13**, **I22** and **I26**) along with gas phase products (CO_2 and NO). Intermediates **I22** and **I26** will be addressed later in this section. It is interesting to note that once FOX-7 passes the three-member ring cyclic transition state

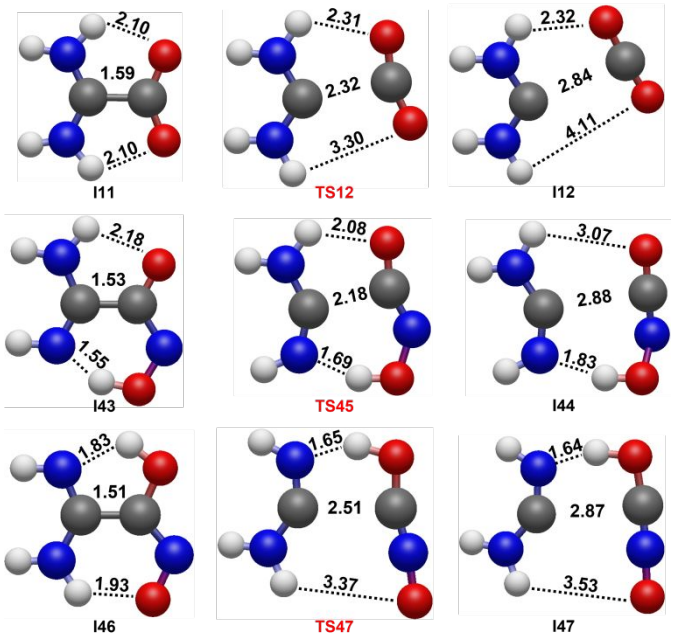

Figure 4 The decomposition mechanism with the bond lengths highlighted in angstrom of Case C, possessing as C-C bond rupture forming hydrogen-bonded post-intermediate. The hydrogen bonds are shown as dashed line.

(**TS11**), there is enough potential energy released to form these low-energy intermediates and gas phase products (e.g., CO_2 and NO).

Instead of forming a three-member ring cyclic transition state, (i.e., **TS11**), the hydrogen in the amine group of **I4** could migrate to the oxygen in the carboxylate group *via* a low barrier of 16 kJ/mol (**TS31**) that is followed by a post-reaction complex (**I31**). Two pathways branch out from **I31** – the first pathway breaks off the hydroxyl (OH) and forms **I34**, which sequentially breaks the C-NO bond and forms **I32** and NO. The second pathway breaks off the N-C bond, leading to **I32** and **I33** (HONO). The former could further break the C-C bond *via* **TS32** and form **I17** and CO, while the latter can break the HO-NO bond and result in HO and NO. Unless specifically mentioned with a TS, all the aforementioned bond breaks are without a transition state. The HO-NO bond breaking in **I33** is the most endothermic (198 kJ/mol), followed by the C-NO bond breaking in **I34** (127 kJ/mol, releasing NO), and C-NO bond breaking in **I32** is the least endothermic (37 kJ/mol, releasing CO). Overall, the potential increases by over 340 kJ/mol following **I31** → **I17** + CO + OH + NO.

As an alternative to **TS31**, the hydrogen in the amine group of **I4** could migrate to the oxygen in the carbonyl group *via* a higher barrier of 63 kJ/mol (**TS21**) which is followed by a post-reaction complex (**I21**). Three pathways branch out from **I21** – the first pathway is initiated by a three-member ring cyclic transition state **TS22** (barrier height = 133 kJ/mol) that results in separated **I22** and NO. **I22** could isomerize to **I26** *via* a swing of the hydroxyl group (**TS23**, barrier height = 64 kJ/mol). Both **I22** and **I26** could break the C-C bond through barrierless dissociation, yielding **I17** along with **I23** and **I24**, respectively. The decomposition of **I17** has been discussed earlier. **I23** and **I24**

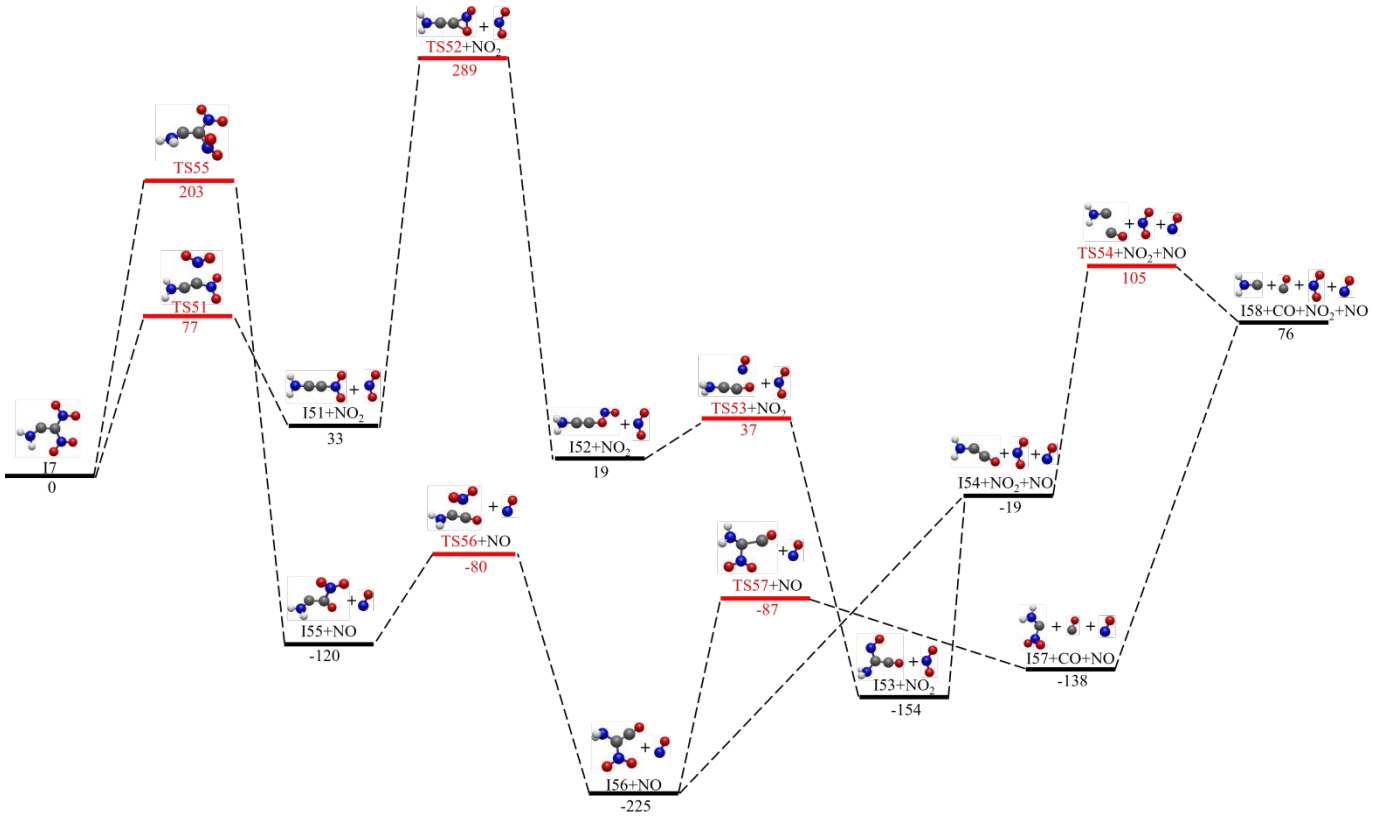

Figure 5 . The potential energy profile of the subsequent decomposition pathways of gas-phase FOX-7 initiated from I7 calculated at the CCSD(T)-F12/VTZ-F12A//M06-2X-D3/Def2-TZVPP + ZPE(M06-2X-D3/Def2-TZVPP) level of theory. Intermediates and products are labelled as "**I**" in black, and the transition states are labelled as "**TS**" in red. The initial decomposed product NH_2 is omitted in this figure, and the potential energy of **I7** is set to zero.

(HOCO) are trans-/cis isomers and close in energy, which could convert to one another *via* transition state **TS27**. **I23**/**I24** could further decompose – take **I23** as an example, it can undergo H-loss and form atomic H and CO_2 in a barrierless dissociation. It is important to note that **I22** could also be formed *via* isomerization of **I11** (H-shift from NH_2 to carboxylate oxygen, **TS15**, barrier height = 19 kJ/mol). Thus, the **TS11** initiated pathway and **TS21** initiated pathway join at **I22**. The second pathway initiated from **I21** is *via* **TS24** (barrier height 57 kJ/mol), which swings the hydrogen in the hydroxyl away from the amine groups, resulting in **I25**. **I25** can form a three-member ring cyclic transition state (**TS25**, barrier height = 131 kJ/mol), which breaks the C-N and O-N bonds simultaneously and form **I26** + NO. Further decomposition of **I26** has been discussed earlier. As the third pathway, the NO_2 group could break off from **I21** and form NO_2 + **I27**. The hydrogen atom in the hydroxyl group of **I27** could swing towards the **NH_2** group, forming a five-member ring structure (**TS26**, barrier height = 8 kJ/mol) before the CO breaks off and form **I13** + CO. Due to the unpaired electron on the carbon of the diamino group, NO_2 could also break off from **I4** *via* beta-scission and form NO_2 + **I28**, which has C_{2v} symmetry. The C-C bond in **I28** can further break *via* a C_s symmetry transition state **TS28** (C-C-O is no longer linear, barrier height = 62 kJ/mol), which also results in **I13** + CO. Similar to the pathways initiated by **TS31**, the pathway initiated by **TS21** also involves many one-step bond dissociations which are highly endothermic as well as some low potential energy intermediates (e.g., **I22** and **I26**) as a result of NO loss *via* the three-member ring cyclic transition states.

B. Subsequent decomposition pathways of (the NH_2 loss product) I7

The potential energy profile of the subsequent decomposition pathways of **I7** is detailed in Figure 5. For clarity, the potential energy of **I7** is set to zero in this figure.

The C-NO_2 bond in **I7** can dissociate to **I51** ($H_2NC{=}CNO_2$) and NO_2 *via* **TS51**. The barrier of this bond rupture is only 77 kJ/mol, much smaller compared to the same process found in **Fox-7** (300 kJ/mol), **I3** (173 kJ/mol), and **I21** (201 kJ/mol). The nitro group at the terminal of **I51** could undergo a nitro-to-nitrite isomerization *via* **TS52**, a three-member ring cyclic structure and accounting for the highest barrier (256 kJ/mol above **I51**) as well as the highest energy (750 kJ/mol above FOX-7) in this study. The IRC calculation of **TS52** locates a stable nitrite intermediate **I52** ($H_2NC{=}CONO$). The potential energy calculation shows that the breaking of the CO-NO bond results in an exothermic reaction (e.g., **I52** → **I54**, ΔH = -38 kJ/mol). This surprising result indicates the CO-NO bond dissociation to be more complicated than a barrierless bond rupture. Transition state search identifies **TS53**, a low barrier (18 kJ/mol above **I52**) shuffling the NO group from the CO side of **I52** to the NH_2 side, which leads to **I53**. An animation showing this process can be found in the Supporting Information (Video file "I52-TS53-I53.mp4"). NO then breaks off from **I53** *via* a barrierless

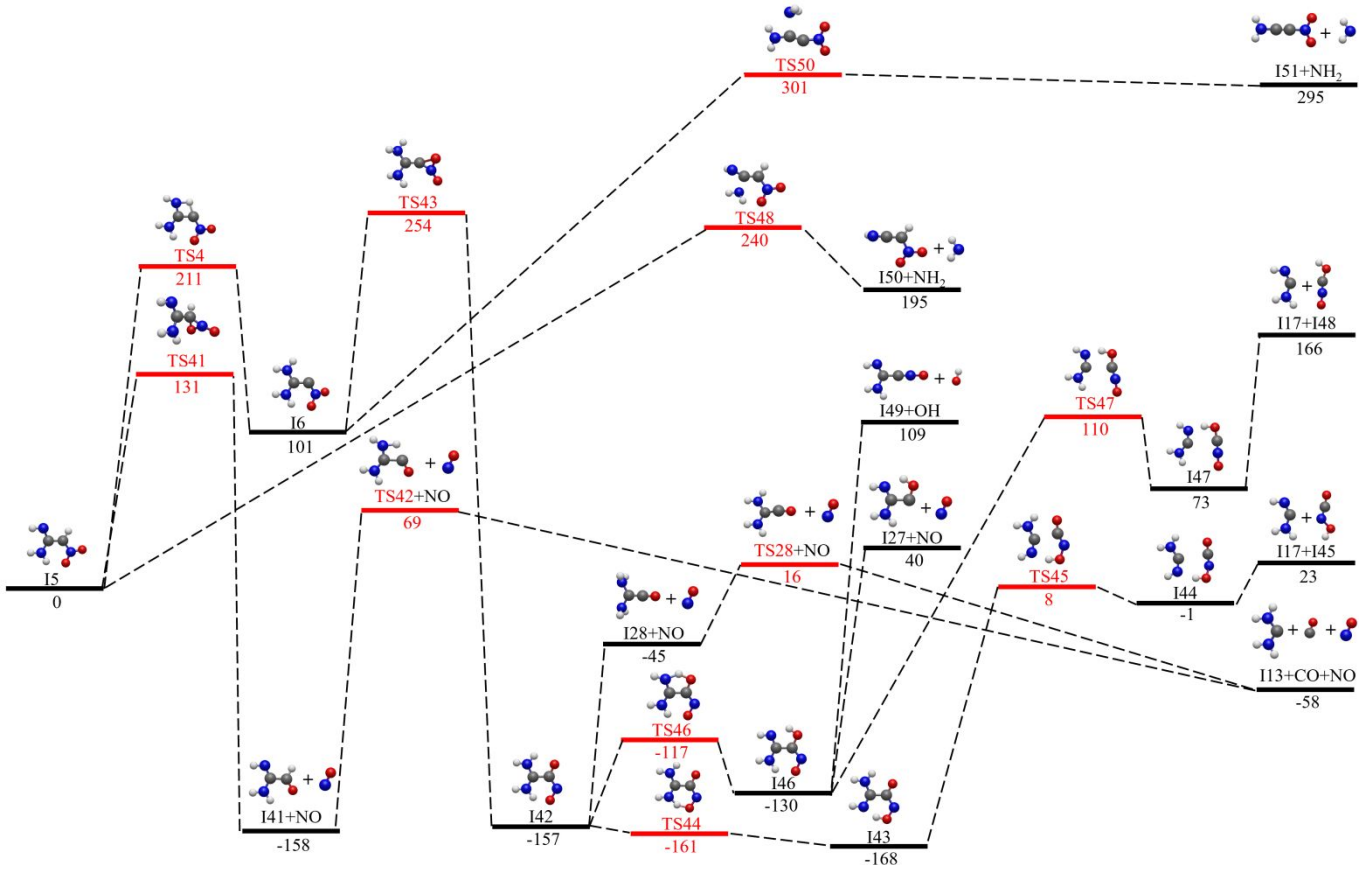

Figure 6 The potential energy profile of the subsequent decomposition pathways of gas-phase FOX-7 initiated from I5 and I6 calculated at the CCSD(T)-F12/VTZ-F12A//M06-2X-D3/Def2-TZVPP + ZPE(M06-2X-D3/Def2-TZVPP) level of theory. Intermediates and products are labelled as "**I**" in black, and the transition states are labelled as "**TS**" in red. The initial decomposed product NO_2 is omitted in this figure, and the potential energy of **I5** is set to zero.

dissociation and forms **I54** (H_2NCCO) + NO. **I54** could eventually dissociate to **I58** (CNH_2) + CO by breaking the C-C bond in **TS54** (124 kJ/mol above **I54**). The major energy barrier of the entire **I7** → **I58 +** CO + NO_2 + NO is the three-member ring nitro-to-nitrite isomerization (**TS52**).

The nitro group near the amine group of **I7** could undergo dissociation *via* the three-member ring cyclic transition states (**TS55**, barrier height = 203 kJ/mol) and form **I55** + NO. The NO_2 group left on **I55** could transit to the NH_2 end of the molecule *via* a low transition state of 40 kJ/mol (**TS56**) and form **I56**. An animation of this process can be found in the Supporting Information (Video file "I55-TS56-I56.mp4"). The newly migrated NO_2 in **I56** could either break free *via* a barrierless dissociation and form **I54** + NO_2, or rupture the C-C bond *via* **TS57** (138 kJ/mol above **I56**) and form **I57** (H_2NCNO_2), which could eventually dissociate to **I58 +** NO_2. Interestingly, the major energy barrier of this pathway is still the three-member ring cyclic transition state (**TS55**) and both pathways (the **TS55** pathway and the **TS51** pathway) initiated from **I7** end up in the same place. We also note that the reaction mechanism of **I55** is very similar to the one reported in **I52**, except that NO (in **I52**), instead of NO_2 (in **I55**), is shuffled from one end of the molecule to the other end before eventually breaks free.

C. Subsequent decomposition pathways of (the NO_2 loss products) I5 and I6

I5 and **I6** have the same chemical formula and can inter-isomerize *via* hydrogen shift (**TS4**), thus they are analyzed together. The potential energy profile of the subsequent decomposition pathways of **I5** and **I6** is detailed in Figure 6. For clarity, the potential energy of **I5** is set to zero.

Starting from **I5**, the dissociation of NO *via* a three-member ring cyclic barrier (**TS41**, barrier height = 131 kJ/mol) is seen again in the formation of **I41** + NO. The hydrogen attached to the carbonyl group of **I41**, which initially belongs to the NH_2 group in FOX-7, can now shift back to the amine side of the molecule while breaking the C-C bond, and form **I13** *via* **TS42** (barrier height = 227 kJ/mol). A similar pathway, **I27** → **TS26** → **I13** + CO, is reported in Figure 3. The further decomposition of **I13** has been discussed in previous sections. The major energy barrier of the entire **I5** → **I13** + CO + NO is once again the three-member ring cyclic transition state (**TS41**). In addition, for **I5**, since the carbon connecting to -NO_2 has an unpaired electron, beta-scission could take place at the C-NH_2 single bond, forming NH_2 and **I50** *via* a barrier of 240 kJ/mol (**TS48**). Starting from **I6**, one of the amine groups on the same side of the nitro group can undergo C-NH_2 bond scission in the beta position with respect to the carbon radical and form NH_2 + **I51** *via* **TS50** (200 kJ/mol above **I6**). Further decomposition of **I51** has been discussed earlier in Figure 5. Like other intermediates with a nitro group, **I6** could also form a three-member ring cyclic transition state (**TS43**, barrier height = 153 kJ/mol) but follows a very different

mechanism in spite of the structural similarity – as noted earlier, most of those three-member ring cyclic transition states break the C-N bond and (either sequentially *vs.* simultaneously) the O-N bond to form gas phase NO – only the O-N bond breaks in **TS43** and leads to a nitroso isomer **I42**. A detailed discussion on this unconventional process will be provided later in the Discussion section. One hydrogen shift (from amine to nitroso oxygen) could take place in **I42** *via* transition state **TS44** forming a more stable intermediate **I43**. We note that **TS44** is a very low transition state, whose *potential energy* is only 4 kJ/mol above **I42**, submerging beneath **I42** after ZPE is included. The cleavage of the C-C bond in **I43** *via* **TS45** (barrier height = 176 kJ/mol) leads to a hydrogen-bond intermediate **I44**, which eventually decomposes into **I17** and **I45**. A similar type of the two-step (C-C breaking followed by hydrogen bond breaking) decomposition mechanism has been previously discussed in the **I4** decomposition pathway (e.g., **I11** → **TS12** → **I12** → **I13** + CO_2, Figure 3). An alternative hydrogen shift (from amine to carbonyl oxygen) could also take place in **I42** *via* transition state **TS46** (barrier height = 40 kJ/mol) forming a less stable intermediate **I46**, which could follow a similar two-step decomposition mechanism to break the C-C bond, **I46** → **TS47** → **I47** → **I17** + **I48**. In addition, **I46** could either break the C-O bond and form **I49** and OH, or break the C-N bond and form **I27** and NO. The nitroso group in **I42** can also possibly dissociate *via* beta-scission processes and form NO + **I28**, which can further break into **I13** + CO. We note this is the same product as the pathway initiated by **TS41**. Overall, except for the **I51** + NH_2 product, the major barriers involved in the aforementioned **I6**/**I5** initiated pathways are three-member ring cyclic transition states (**TS41**) and its hydrogen-shifted lookalike (**TS43**).

IV. Discussion

The CO-NO bond rupture from **I1** to products (**I4** + NO) has been regarded as a barrierless process for decades.[14,18,19] A recent study[25] carried out at B2PLYP/6-31G(d,p) level of theory reports that the CO-NO bond rupture could be accomplished *via* a loosely-bonded TS of 43 kJ/mol (Figure 4 in Guan et al.[25]). After the TS, the NO radical in the post-reaction complex, $O_2NC(O)C(NH_2)NH\cdots H\cdots NO$, interacts with the amine group through a hydrogen bond at a distance of 2.284 Å and with the carbonyl group by radical-radical adduct at 2.808 Å apart. This hydrogen-bonded radical-radical complex lies below the dissociation products by 9 kJ/mol. The author also performed a potential energy scan for the CO-NO bond of **I1** between 1.50 and 4.00 Å with other geometrical parameters constrained. The highest potential energy along this scan is about 25 kJ/mol above **I1**. While it is certainly possible that the $O_2NC(O)C(NH_2)NH\cdots H\cdots NO$ pathway is valid in the sense that it breaks the CO-NO bond, the energy scan suggests that the lowest barrier of the such process should be no larger than 25 kJ/mol. This is due to the fact that the rest of the geometries are not allowed to relax during the energy scan of a bond.[25] In order to search for the lowest barrier, multiple restrained optimizations are carried out, in which the CO-NO bond is held at discrete, fixed distances between 1.40 and 10.00 Å with a 0.100 Å increment, while the rest of the molecules are optimized. The calculation shows that the potential energy *monotonically* increases by 3 kJ/mol as the CO-NO bond breaks and the geometry gradually shifts from **I1** to **I4** + NO, confirming a barrierless dissociation path. The 3 kJ/mol potential energy difference is well below the maximally allowed 25 kJ/mol. Although the focus has been mostly on the lowest energy path, as it is the most relevant concerning the kinetics of the chemical reaction, it is also important to note that there could be multiple valid pathways that exist between two species. The CO-NO bond rupture could serve as one of such examples – the NO group of the nitrite in **I1** could swing towards the nitro group (**TS2**, barrier height = 35 kJ/mol), followed by a post-TS intermediate **I2**, before dissociating to **I4** + NO.

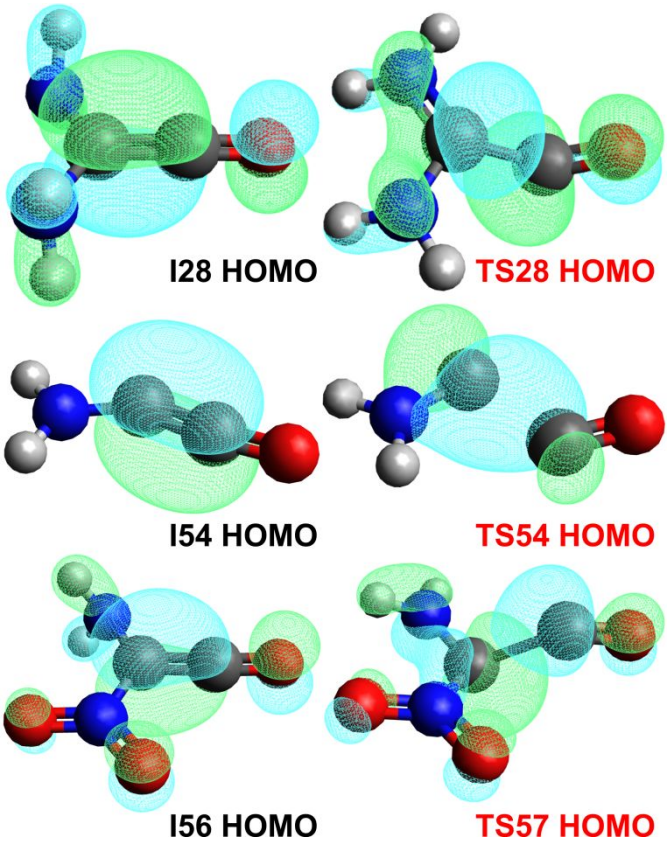

Figure 7 The highest occupied molecular orbitals (HOMO) of I28, I54, and I56 and their corresponding transition states.

There are three different mechanisms of C-C bond rupture found in various intermediates, which can be categorized into three cases: A). barrierless dissociation, B). dissociation with a barrier (TS), and C). dissociation with a TS and a post-TS intermediate. Case A includes the C-C bond rupture in **I22** and **I23**. There are no unpaired electrons on either of the carbon and this bond resembles a normal sigma C-C single bond (BO = 0.96) with their bond length of 1.530 Å. The bond breaks in one step with the large endothermicity, (e.g., 413 kJ/mol and 396 kJ/mol for **I22** and **I26**, respectively) close to the bond energy of a sigma C-C single bond. Case B includes **I27**, **I28, I32**, **I41**, **I54**, and **I56**, whose barrier of dissociation can also be readily correlated to the chemical bonding theories. The C-C bond in the first three intermediates differ in electron pulling groups on the C-O side.

For **I27**, there are *two* unpaired electrons on the carbon connecting the hydroxyl, making the C-C bond (BO = 0.78) very unstable – **TS26** responsible for this bond breaking is only 8 kJ/mol. For **I32**, the carboxyl carbon has *one* unpaired electron, and the C-C bond (BO = 0.81) is stronger than the one in **I27**, with a barrier (**TS32**) of 59 kJ/mol. There is no unpaired electron in the case of **I41**, thus it possesses the strongest C-C bond (BO = 0.93) among the three, with a barrier (**TS42**) of 227 kJ/mol. **I28**, **I54** and **I56** (Figure 7), in which the central carbon forms a double bond ($\sigma + \pi$) with carbonyl carbon, could dissociate the C-CO bond *via* a bending motion – the π orbitals changing from in-phase to out-of-phase, as the C-CO bond bends towards their corresponding TSs instead of C-C bond stretching. Case C possesses an interesting stepwise mechanism for the C-C bond rupture, as it possesses a post-TS intermediate, which includes

1) **I11** → **TS12** (barrier height = 55 kJ/mol) → **I12** → **I13** + CO_2
2) **I43** → **TS45** (barrier height = 176 kJ/mol) → **I44** → **I17** + **I45**
3) **I46** → **TS47** (barrier height = 240 kJ/mol) → **I47** → **I17** + **I48**

All three intermediates first go across a TS that dissociates the C-C bonds, but instead of just breaking the molecules into two halves, a hydrogen bond complex could be formed as a post-TS intermediate. The difference in the barrier heights could be interpreted with a similar argument as discussed in the previous two cases. It is also of interest to note that in all three pathways of case C, the potential energy of the transition state is lower than the separated species. Nonetheless, the impact on reaction dynamics caused by a submerged barrier and/or hydrogen-bonded intermediate should not be ignored. For example, a submerged barrier is detected in a recent chemical dynamics study of the bimolecular collision of HBr^+ + CO_2 and the reaction is largely indirect (trapped by $[BrH\cdots OCO]^+$ and/or $[Br\cdots HOCO]^+$ intermediates) – under different excitations (collision, rotation, etc.), the dynamics of the reaction changes vastly.[56] Therefore, it would be interesting to investigate how the submerged barrier would impact the dynamics of the C-C bond dissociation of these intermediates with *ab initio* molecular dynamics in the future. The structures of these case C intermediates are shown in Figure 4 with the C-C and hydrogen bond lengths highlighted.

As noted earlier, the C-N-O three-member ring cyclic transition state accounts for the major barrier in almost all pathways. One of such examples is **TS1**, a barrier 273 kJ/mol above FOX-7 – Once passed, it could release up to 291 kJ/mol potential energy along with **I4** and NO, which is more than enough to drive further decomposition and form gas-phase products such as CO_2 (**TS12**, -93 kJ/mol with respect to FOX-7), H_2 (**TS13**, 151 kJ/mol with respect to FOX-7), and additional NO (**TS11**, 151 kJ/mol with respect to FOX-7). The TSs featuring a three-member ring of C-N-O could lead to three different cases – A). break the C-N bond and lead to nitro-to-nitrite isomerization, such as **TS1** and **TS52**; B). break the C-N and O-N bonds simultaneously and release NO, including **TS11**, **TS22**, **TS25**, **TS41**, and **TS55**; and C). as the only example in this study, **TS43** breaks the O-N bond and leads to nitro-to-nitroso isomerization. A picture comparing the first two major processes is provided in Figure 8. There are two characteristics of these TSs that are important to the decomposition dynamics

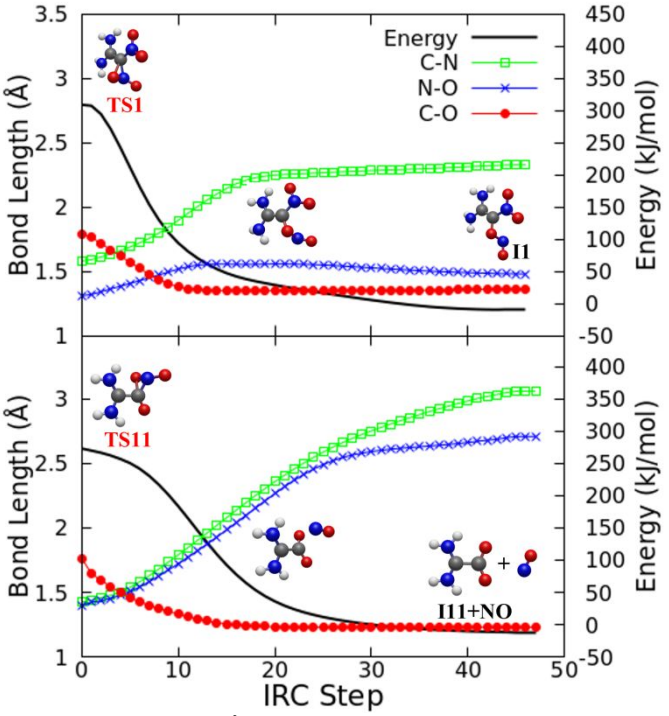

Figure 8 The bond lengths in Å and potential energy change in kJ/mol along with IRC steps of the C-N-O three-member ring cyclic transition state. The representative pathways of two major mechanisms (nitro-to-nitrite isomerization and NO dissociation) are shown in the top and bottom figures, respectively.

of FOX-7. The first characteristic is the height of the barriers. If the primary and secondary decompositions are considered as the early stage of FOX-7 decomposition, then these barriers involved in the early stage lie between 151 kJ/mol (**TS11**) and 289 kJ/mol (**TS52**) – moderate to high barriers provide the stability of FOX-7 as an energetic material. The second characteristic is that compared to the pre-TS complex (nitro), more potential energy is released after crossing the TS in all three different cases. The large potential energy difference between the TS and A). nitrite, B). intermediate + NO, and C). nitroso indicates that once the initial three-member ring forms (i.e., the TS is passed), large potential energy is released and consecutive decompositions become spontaneous. The second characteristic is what makes FOX-7 an energetic material.

V. Conclusions

The decomposition pathways of FOX-7 in the gas phase identified in this manuscript are indicative of the reaction mechanism of the decomposition in the condensed phase. As noted in a previous study[19] where the potential energy profile of the decomposition of FOX-7 in the gas phase is compared to its counterpart in the condensed phase – although the overall shapes of the potential energy profiles are similar, the condensed phase could potentially impact the decomposition in two ways: the first is that as a result of the crystal, FOX-7 is in a distorted configuration as compared to the structure optimized in the gas phase (thus increase potential energy) and the second is that the distorted structure is stabilized *via* intermolecular

hydrogen bonds (thus decrease potential energy). The decomposition of FOX-7 in the condensed phase navigates under these two conflicting effects – for example, the height of the initial nitro-to-nitrite TS (**TS1**) decreases and the hydrogen transfer TS (**TS3**) increases, which is due to the number of intermolecular hydrogen bond disrupted/reformed in the process of transiting from an intermediate to the corresponding TS.[19] This conclusion is made in the early stage of the decomposition, i.e., when the structure of the crystal still largely holds, as indicated by the spectroscopy results.

As Figure 1 indicates, the decomposition of FOX-7 consists of a large number of pathways that involve numerous gas-phase products. Those structures that are close to the FOX-7 in Figure 1 are impacted more by the encapsulated environment (i.e., condensed phase), but among them, the three-member ring cyclic transition states are key components driving the early stage of the decomposition. Once the early stage has passed and enough potential energy has been released, the crystal structure breaks down, at which point, the gas phase dynamics dominates. The results also suggest that the nitro groups, compared to the amine groups, are more responsible for the stability and the potential energy release (e.g., detonation) of gas phase FOX-7. However, it should be noted that in the context of the condensed phase, the nitro and amine groups form intermolecular hydrogen bonds, thus both play a role in the decomposition dynamics.

Author Contributions

Yuheng Luo: Methodology, Formal analysis, Writing – original draft, Investigation, Visualization. Christopher Kang: Visualization, Writing - review & editing. Ralf I. Kaiser: Conceptualization, Writing - review & editing. Rui Sun: Supervision, Conceptualization, Writing - original draft.

Conflicts of interest

There are no conflicts to declare.

Acknowledgements

The research reported in this manuscript is supported by the Army Research Office (grant number: A9550-21-1-0221). The authors appreciate the Information Technology Service (ITS) from the University of Hawaii at Manoa for the computational resources.

Notes and references

1 H. H. Krause, *New Energetic Materials*, 2004.
2 G. D. Kozak, Factors Augmenting the Detonability of Energetic Materials, *Propellants Explos. Pyrotech.*, 2005, **30**, 291–297.
3 R. P. Singh, R. D. Verma, D. T. Meshri and J. M. Shreeve, Energetic nitrogen-rich salts and ionic liquids, *Angew. Chem. - Int. Ed.*, 2006, **45**, 3584–3601.
4 A. J. Bellamy, in *Structure and Bonding*, ed. T. M. Klapötke, Springer Berlin Heidelberg, Berlin, Heidelberg, 2007, vol. 125, pp. 1–33.
5 T. M. Klapötke, *Chemistry of High-Energy Materials*, De Gruyter, 2019.
6 N. V. Latypov, J. Bergman, A. Langlet, U. Wellmar and U. Bemm, Synthesis and reactions of 1,1-diamino-2,2-dinitroethylene, *Tetrahedron*, 1998, **54**, 11525–11536.
7 S. N. Bulusu, Ed., *Chemistry and Physics of Energetic Materials*, Springer Netherlands, Dordrecht, 1990.
8 P. F. Pagoria, *Synthesis of pure RDX*, 1994.
9 H. Östmark, H. Bergman, K. Ekvall and A. Langlet, A study of the sensitivity and decomposition of 1,3,5-trinitro-2-oxo-1,3,5-triazacyclo-hexane, *Thermochim. Acta*, 1995, **260**, 201–216.
10 H. Dorsett Defence Science and Technology Organisation (Australia), Aeronautical and Maritime Research Laboratory (Australia). Weapons Systems Division. *Computational studies of FOX-7, a new insensitive explosive*, DSTO Aeronautical and Maritime Research Laboratory, Salisbury, S. Aust., 2000.
11 W. Trzciński and A. Belaada, 1,1-Diamino-2,2-dinitroethene (DADNE, FOX-7) – Properties and Formulations (a Review), *Cent. Eur. J. Energ. Mater.*, 2016, **13**, 527–544.
12 T. L. Jensen, E. Unneberg and T. E. Kristensen, Smokeless GAP-RDX Composite Rocket Propellants Containing Diaminodinitroethylene (FOX-7), *Propellants Explos. Pyrotech.*, 2017, **42**, 381–385.
13 P. Politzer, M. C. Concha, M. E. Grice, J. S. Murray, P. Lane and D. Habibollazadeh, Computational investigation of the structures and relative stabilities of amino/nitro derivatives of ethylene, *J. Mol. Struct. THEOCHEM*, 1998, **452**, 75–83.
14 A. Gindulytè, Proposed mechanism of 1,1-diamino-dinitroethylene decomposition: A density functional theory study, *J. Phys. Chem. A*, 1999, **103**, 11026–11033.
15 A. V. Kimmel, P. V. Sushko, A. L. Shluger and M. M. Kuklja, Effect of charged and excited states on the decomposition of 1,1-diamino-2,2-dinitroethylene molecules, *J. Chem. Phys.*, 2007, **126**, 234711.
16 B. Yuan, Z. Yu and E. R. Bernstein, Initial decomposition mechanism for the energy release from electronically excited energetic materials: FOX-7, *J Chem Phys*, 2014, **140**, 74708.
17 R. S. Booth and L. J. Butler, Thermal decomposition pathways for 1,1-diamino-2,2-dinitroethene (FOX-7), *J. Chem. Phys.*, 2014, **141**, 134315.
18 V. G. Kiselev and N. P. Gritsan, Unexpected Primary Reactions for Thermolysis of 1,1-Diamino-2,2-dinitroethylene (FOX-7) Revealed by *ab Initio* Calculations, *J. Phys. Chem. A*, 2014, **118**, 8002–8008.
19 A. M. Turner, Y. Luo, J. H. Marks, R. Sun, J. T. Lechner, T. M. Klapötke and R. I. Kaiser, Exploring the Photochemistry of Solid 1,1-Diamino-2,2-dinitroethylene (FOX-7) Spanning Simple Bond Ruptures, Nitro-to-Nitrite Isomerization, and Nonadiabatic Dynamics, *J. Phys. Chem. A*, 2022, **126**, 4747–4761.
20 J. P. Perdew, Density-functional approximation for the correlation energy of the inhomogeneous electron gas, *Phys. Rev. B*, 1986, **33**, 8822–8824.
21 A. D. Becke, Density-functional thermochemistry. III. The role of exact exchange, *J. Chem. Phys.*, 1993, **98**, 5648–5652.
22 R. Krishnan, J. S. Binkley, R. Seeger and J. A. Pople, Self-consistent molecular orbital methods. XX. A basis set for correlated wave functions, *J. Chem. Phys.*, 1980, **72**, 650–654.
23 A. D. Becke, Density-functional exchange-energy approximation with correct asymptotic behavior, *Phys. Rev. A*, 1988, **38**, 3098–3100.
24 L. A. Curtiss, P. C. Redfern and K. Raghavachari, Gaussian-4 theory, *J. Chem. Phys.*, 2007, **126**, 084108.

25 Y. Guan, X. Zhu, Y. Gao, H. Ma and J. Song, Initial Thermal Decomposition Mechanism of $(NH_2)_2C{=}C(NO_2)(ONO)$ Revealed by Double-Hybrid Density Functional Calculations, *ACS Omega*, 2021, **6**, 15292–15299.
26 Chr. Møller and M. S. Plesset, Note on an Approximation Treatment for Many-Electron Systems, *Phys. Rev.*, 1934, **46**, 618–622.
27 N. X. Wang and A. K. Wilson, The behavior of density functionals with respect to basis set. I. The correlation consistent basis sets, *J. Chem. Phys.*, 2004, **121**, 7632.
28 E. Sim, S. Song and K. Burke, Quantifying Density Errors in DFT, *J. Phys. Chem. Lett.*, 2018, **9**, 6385–6392.
29 T. B. Adler, G. Knizia and H.-J. Werner, A simple and efficient CCSD(T)-F12 approximation, *J. Chem. Phys.*, 2007, **127**, 221106.
30 U. Bemm and H. Östmark, 1,1-Diamino-2,2-dinitroethylene: a Novel Energetic Material with Infinite Layers in Two Dimensions, *Acta Crystallogr. C*, 1998, **54**, 1997–1999.
31 S. N. Rashkeev, M. M. Kuklja and F. J. Zerilli, Electronic excitations and decomposition of 1,1-diamino-2,2-dinitroethylene, *Appl. Phys. Lett.*, 2003, **82**, 1371–1373.
32 A. Hu, B. Larade, H. Abou-Rachid, L.-S. Lussier and H. Guo, A First Principles Density Functional Study of Crystalline FOX-7 Chemical Decomposition Process under External Pressure, *Propellants Explos. Pyrotech.*, 2006, **31**, 355–360.
33 Q. Wu, W. Zhu and H. Xiao, DFT study on crystalline 1,1-diamino-2,2-dintroethylene under high pressures, *J. Mol. Model.*, 2013, **19**, 4039–4047.
34 Y. Zhao and D. G. Truhlar, The M06 suite of density functionals for main group thermochemistry, thermochemical kinetics, noncovalent interactions, excited states, and transition elements: two new functionals and systematic testing of four M06-class functionals and 12 other function, *Theor. Chem. Acc.*, 2008, **120**, 215–241.
35 F. Weigend and R. Ahlrichs, Balanced basis sets of split valence, triple zeta valence and quadruple zeta valence quality for H to Rn: Design and assessment of accuracy, *Phys. Chem. Chem. Phys.*, 2005, **7**, 3297.
36 M. Valiev, E. J. Bylaska, N. Govind, K. Kowalski, T. P. Straatsma, H. J. J. Van Dam, D. Wang, J. Nieplocha, E. Apra, T. L. Windus and W. A. de Jong, NWChem: A comprehensive and scalable open-source solution for large scale molecular simulations, *Comput. Phys. Commun.*, 2010, **181**, 1477–1489.
37 K. Fukui, Formulation of the reaction coordinate, *J. Phys. Chem.*, 1970, **74**, 4161–4163.
38 J. Ischtwan and M. A. Collins, Determination of the intrinsic reaction coordinate: Comparison of gradient and local quadratic approximation methods, *J. Chem. Phys.*, 1988, **89**, 2881–2885.
39 S. Maeda, Y. Harabuchi, Y. Ono, T. Taketsugu and K. Morokuma, Intrinsic reaction coordinate: Calculation, bifurcation, and automated search, *Int. J. Quantum Chem.*, 2015, **115**, 258–269.
40 Y. Luo, T. Kreuscher, C. Kang, W. L. Hase, K.-M. Weitzel and R. Sun, A chemical dynamics study of the HCl + HCl+ reaction, *Int. J. Mass Spectrom.*, 2021, **462**, 116515.
41 K. Fujioka, K.-M. Weitzel and R. Sun, The Potential Energy Profile of the HBr^+ + HCl Bimolecular Collision, *J. Phys. Chem. A*, 2022, **126**, 1465–1474.
42 A. E. Reed, R. B. Weinstock and F. Weinhold, Natural population analysis, *J. Chem. Phys.*, 1985, **83**, 735–746.
43 A. E. Reed, L. A. Curtiss and F. Weinhold, Intermolecular interactions from a natural bond orbital, donor-acceptor viewpoint, *Chem. Rev.*, 1988, **88**, 899–926.
44 E. D. Glendening and F. Weinhold, Natural resonance theory: II. Natural bond order and valency, *J. Comput. Chem.*, 1998, **19**, 610–627.
45 A. J. Bridgeman, G. Cavigliasso, L. R. Ireland and J. Rothery, The Mayer bond order as a tool in inorganic chemistry†, *J. Chem. Soc. Dalton Trans.*, 2001, 2095–2108.
46 T. Lu and F. Chen, Multiwfn: A multifunctional wavefunction analyzer, *J. Comput. Chem.*, 2012, **33**, 580–592.
47 K. Raghavachari, G. W. Trucks, J. A. Pople and M. Head-Gordon, A fifth-order perturbation comparison of electron correlation theories, *Chem. Phys. Lett.*, 1989, **157**, 479–483.
48 K. A. Peterson, T. B. Adler and H.-J. Werner, Systematically convergent basis sets for explicitly correlated wavefunctions: The atoms H, He, B–Ne, and Al–Ar, *J. Chem. Phys.*, 2008, **128**, 084102.
49 G. Knizia, T. B. Adler and H.-J. Werner, Simplified CCSD(T)-F12 methods: Theory and benchmarks, *J. Chem. Phys.*, 2009, **130**, 054104.
50 H.-J. Werner, P. J. Knowles, G. Knizia, F. R. Manby and M. Schütz, Molpro: a general-purpose quantum chemistry program package, *Wiley Interdiscip. Rev. Comput. Mol. Sci.*, 2012, **2**, 242–253.
51 H.-J. Werner, P. J. Knowles, F. R. Manby, J. A. Black, K. Doll, A. Heßelmann, D. Kats, A. Köhn, T. Korona, D. A. Kreplin, Q. Ma, T. F. Miller, A. Mitrushchenkov, K. A. Peterson, I. Polyak, G. Rauhut and M. Sibaev, The Molpro quantum chemistry package, *J. Chem. Phys.*, 2020, **152**, 144107.
52 T. B. Adler and H.-J. Werner, An explicitly correlated local coupled cluster method for calculations of large molecules close to the basis set limit, *J. Chem. Phys.*, 2011, **135**, 144117.
53 K. E. Yousaf and K. A. Peterson, Optimized auxiliary basis sets for explicitly correlated methods, *J. Chem. Phys.*, 2008, **129**, 184108.
54 T. H. Dunning, Gaussian basis sets for use in correlated molecular calculations. I. The atoms boron through neon and hydrogen, *J. Chem. Phys.*, 1989, **90**, 1007–1023.
55 A. J. C. Varandas, Basis-set extrapolation of the correlation energy, *J. Chem. Phys.*, 2000, **113**, 8880–8887.
56 Y. Luo, K. Fujioka, A. Shoji, W. L. Hase, K.-M. Weitzel and R. Sun, Theoretical Study of the Dynamics of the HBr + + CO 2 → HOCO + + Br Reaction, *J. Phys. Chem. A*, 2020, **124**, 9119–9127.